Progress In Electromagnetics Research, Vol. 124, 285–299, 2012

A MULTI-BEAM AND MULTI-RANGE RADAR WITH FMCW AND DIGITAL BEAM FORMING FOR AUTOMOTIVE APPLICATIONS

S.-H. Jeong [1, *], H.-Y. Yu [1], J.-E. Lee [1], J.-N. Oh [1], and K.-H. Lee [2]

[1]Department of Radar Research & Development, MANDO Electronics Laboratory, Seongnam-si, Gyeonggi-do 463-870, Korea

[2]Department of Electronic Engineering, Sogang University, 35 Baekbeom-ro, Mapo-gu, Seoul 121-742, Korea

Abstract—In this paper, we propose a multi-beam and multi-range (MBMR) radar with frequency modulated continuous wave (FMCW) waveform and digital beam forming (DBF) algorithm to cover a detection area of long range and narrow angle (150 m, $\pm 10^\circ$) as well as short range and wide angle (60 m, $\pm 30^\circ$) as a single 24 GHz sensor. The developed radar is highly integrated with multiple phased-array antennas, a two-channel transmitter and a four-channel receiver using K-band GaAs RF ICs, and back-end processing board with subspace-based DBF algorithm. The proposed 24 GHz MBMR radar can be used for an adaptive cruise control (ACC) stop-and-go system which typically consists of three radars, such as two 24 GHz short-range radars for object detection in an adjacent lane and one 77 GHz long-range radar for object detection in the center lane.

1. INTRODUCTION

According to the statistics, it is reported that more than 160 thousand people lose their lives and more than 6 million people have been injured because of car accidents all over the world annually [1]. Nowadays, lots of researchers working for automotive application have been trying to develop the radar sensors for reducing human casualties from those collision accidents [2–7]. As the result of this market demand, various radar systems, such as adaptive cruise control (ACC), stop-and-go, blind spot detection (BSD), lane change assist (LCA), and rear crash

Received 8 November 2011, Accepted 18 January 2012, Scheduled 25 January 2012

* Corresponding author: Seong-Hee Jeong (erjsh@mando.com).

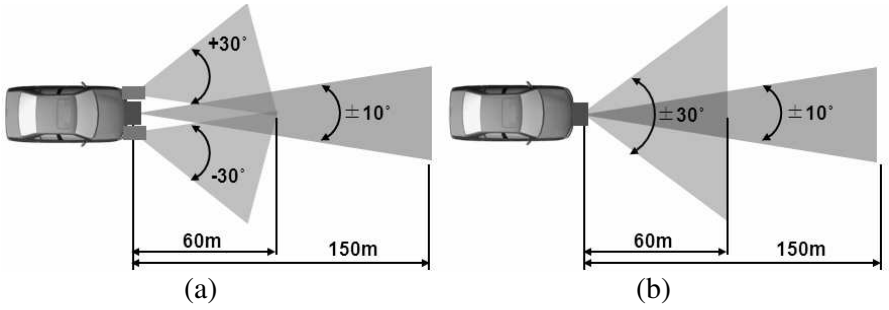

Figure 1. (a) A typical ACC stop-and-go system. (b) A new ACC stop-and-go system using the proposed MBMR radar.

warning (RCW), have been widely applied to vehicles. Particularly, an ACC stop-and-go system that has not only ACC function but also stop-and-go function to mitigate or prevent collision accidents in the emergency situation of frontal target vehicles, is an important safety application.

Figure 1(a) shows a typical ACC stop-and-go system that requires three radar sensors: two short range radars with a range coverage of 60 m and an angle coverage up to $\pm 30^\circ$ to detect cut-in or cut-out targets in an adjacent lane, and one more long range radar with a coverage of 150 m and $\pm 10^\circ$ to detect vehicles in the center lane [8]. To implement such an ACC stop-and-go system, radar suppliers have developed various radar sensors. A 77 GHz radar of DENSO corporation presents a switching array structure with DBF technology. This radar has a range detection capability of 150 m and an angle detection capability of $\pm 10^\circ$ [9]. The company BOSCH also has developed a 77 GHz ACC radar with a range detection capability up to 250 m and an angle detection capability of $\pm 15^\circ$. HELLA and M/A-COM present 24 GHz short-range radars with a simple mono-pulse structure. These short range radars have a range detection capability of 70 m and an angle detection capability of more than 30° [10, 11]. However, these bulky radar sensors have a spatial limitation in the aspect of frontal bumper installation and make the cost of an ACC stop-and-go system high. In order to reduce the size and cost of these bulky radar systems, a single sensor based 24 GHz radar with a one-channel transmitter and four-channel receiver was developed [12]. However, the single beam radar with only one-channel transmitter is difficult to discriminate a primary vehicle in the center lane and vehicles in an adjacent lane in dense traffic situation.

In this paper, to overcome limitations of both bulky ACC stop-

and-go system with three radar sensors and discrimination capability for a primary vehicle detection in dense traffic situation, we designed a single sensor based MBMR radar that has two switching array antennas to cover long range and narrow angle coverage (150 m, $\pm 10^\circ$) and short range and wide angle coverage (60 m, $\pm 30^\circ$) respectively as shown in Figure 1(b). The proposed MBMR radar uses an FMCW waveform as the signal source, which has a simple architecture and requires low computing power compared to a pulse waveform [13–20]. The FMCW waveform is used to obtain the range and velocity simultaneously. Also, the radar adopts subspace based DBF technology using a switching array structure with multi-channel transmitter and receiver to implement multi-beam and multi-range function. This switching array structure can lower the system cost by reducing the number of receiver channels, as well as lessen the system size. The DBF technology is used to detect the azimuth angle with high resolution and accuracy [21–26].

This paper is organized as follows. In Section 2, the system design concept of the proposed MBMR radar regarding hardware structure, FMCW waveform and DBF algorithm are given. In Section 3, the design results of front-end and back-end modules are described. In Section 4, experimental results and discussion in the aspect of detection performance are presented.

2. RADAR SYSTEM DESIGN

2.1. Hardware Structure Design

In order to implement multi-detection function for range and angle of targets as a single sensor, a two-channel transmitter (TX) and a four-channel receiver (RX) structure is proposed as shown in Figure 2. To reduce the size and cost of the complex transceiver with multi-channels, we used single-pole double-throw (SPDT) and single-pole four-throw (SP4T) switches for the TX and RX, respectively.

The TX port #1 for long range and narrow angle detection (150 m, $\pm 10^\circ$) is connected to multiple series-fed patch antennas (SFPAs). The TX port #2 for short range and wide angle detection (60 m, $\pm 30^\circ$) uses a single SFPA. The proposed SFPAs have advantages, such as light weight, low profile, and a compact line length feed network [27]. To obtain desired radiation pattern and gain within limited radar size, a patch of 12 is used as one array configuration. However, the array configuration with the same patch size shows poor side-lobe level (SSL) performance. To improve the SSL performance, the patch widths as shown in Figure 3 are optimized by a 3D simulator. A coaxial feeding

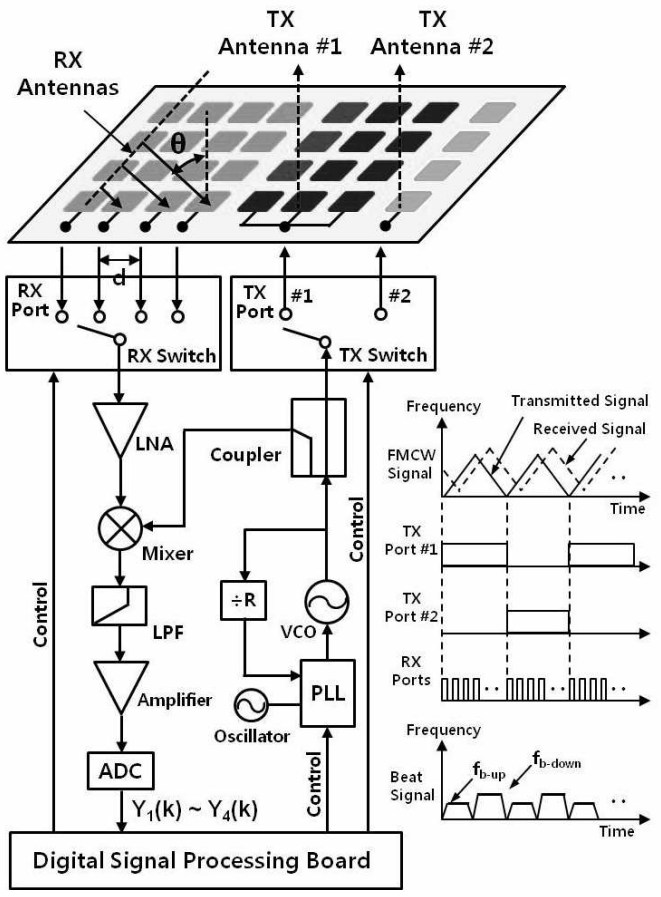

Figure 2. System block diagram of a MBMR radar.

is applied to the center point of patch array by considering an effective connection between the RF module and the antennas.

The TX consists of two-port SFPAs, a SPDT switch, a coupler, a voltage controlled oscillator (VCO), and a fractional N frequency synthesizer. The coupler is used for dividing VCO power to the TX output and mixer LO ports. The designed coupler has the coupled line configuration, which can control coupling power by line width and length. Normally, the FMCW signal is generated by the direct digital synthesizer (DDS), which features remarkable frequency resolution, low spurious output, and direct implementation of frequency, phase and amplitude modulation. However, the DDS has a bulky size and high cost. To mitigate this problem, the fractional synthesizer with an

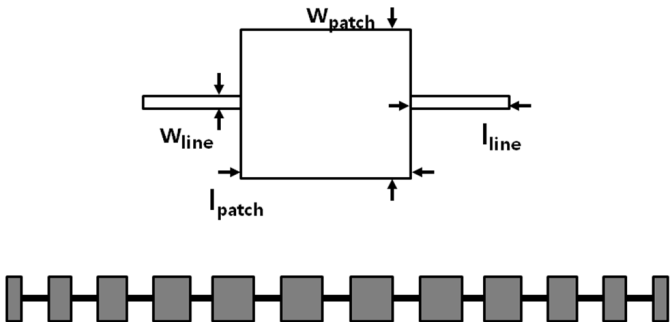

Figure 3. Single patch and array configurations of SFPA.

advanced delta-sigma modulator that gives highly fine step size and low spurious output is used for the proposed radar system [28]. The synthesizer provides low enough spurious output, which can remove the need for DDS references.

The RX has four SFPAs, a SP4T switch, a low noise amplifier (LNA), a mixer, a low pass filter (LPF), an intermediate frequency (IF) amplifier, and an analog-to-digital converter (ADC). The switch configuration can deteriorate the noise figure performance of the RX, if the switch is placed on the first stage of the RX. To achieve a low noise figure of the RX, the switch is followed by the LNA, which has a low noise figure of 2.5 dB and a high gain of 23.5 dB. Such high gain can reduce the noise figure effect of the mixer. So the noise figure of the RX has almost the same value with the loss of the switch. The LPF plays an important role to determine the noise bandwidth of the RX, which affects a minimum detectable power. The bandwidth is determined by the highest beat frequency which is calculated by maximum range and maximum Doppler frequency.

The timing diagram for the TX and RX ports is also shown in Figure 2. The TX port #1 generates a FMCW signal of 1 period, which consists of up-chirp and down-chirp. During that time, the TX port #2 is in the off-state and the RX port is switched at stated intervals. For the next period of the FMCW signal, the TX port #2 is in the on-state, the TX port #1 is off-state and the RX port is switched at stated intervals. Such operation is repeated in order for the on-state of the radar. The received beat signals according to the FMCW waveform are shown in Figure 2.

The back-end processing module performs digital signal processing such as linear control of FMCW waveform, coherent sampling of received beat signals, preprocessing for subspace based DBF and peak

detection in frequency domain, postprocessing for data association, track filtering, path prediction, target selection, and longitudinal control of target vehicle.

2.2. Waveform and DBF Algorithm Design

In order to extract the radial velocity and range information of various targets on the road, we used the FMCW waveform as shown in Figure 2. Its center frequency is 24.1 GHz. The frequency sweep bandwidth is 100 MHz and chirp period is 2 ms. A sampling frequency of Rx switch is 1 MHz, which means a sampling frequency of each Rx channel is under 250 kHz. When the reflected received signals are mixed with transmitted signals, the beat signals are given by

$$f_{b\text{-}up} = |f_r - f_d| \tag{1}$$

$$f_{b\text{-}down} = |f_r + f_d| \tag{2}$$

where f_r is the range Doppler frequency and f_d is velocity Doppler frequency. Accordingly, the relative range and velocity of the target can be calculated by

$$R = \frac{f_r cT}{2B} \tag{3}$$

$$V = \frac{f_d \lambda}{2} \tag{4}$$

where c is the velocity of light, T is the period of each chirp, B is the transmitted bandwidth, and λ is wave length.

In order to extract exact angle information with high resolution compared to conventional beam forming [29], we designed the subspace-based DBF algorithm with multiple signal classification (MUSIC) [30–35]. Receiver array geometries of implemented radar

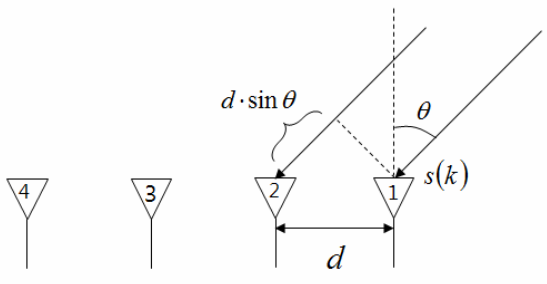

Figure 4. Geometric representation of receiver array.

system are depicted in Figure 4. The signal model in the proposed array radar is defined by

$$\mathbf{Y}(k) = \mathbf{A}(\theta)\mathbf{s}(k) + \mathbf{n}(k) \tag{5}$$

where $\mathbf{A}(\theta) = \lceil \mathbf{a}(\theta_1), \mathbf{a}(\theta_2), \ldots, \mathbf{a}(\theta_M) \rceil$, $\mathbf{a}(\theta)$ is a (4×1) steering vector, M is the number of the target signal source, $\mathbf{s}(k)$ is a desired signal vector, $\mathbf{Y}(k)$ is the received baseband signal vector as shown in Figure 2, and $\mathbf{n}(k)$ is additive noise signal. The interval d between each receiver antenna is uniform at 0.5λ to achieve wide angle detection of more than $\pm 30^\circ$ by reducing the grating lobe during the angle steering. The spatial covariance matrix of 4 channel received signals can be obtained by

$$\mathbf{R} = E\left\{\mathbf{Y}(k)\mathbf{Y}^H(k)\right\} = \mathbf{A}E\left\{\mathbf{s}(k)\mathbf{s}^H(k)\right\}\mathbf{A}^H + E\left\{\mathbf{n}(k)\mathbf{n}^H(k)\right\} \tag{6}$$

where $E\{\cdot\}$ denotes statistical expectation. An estimate of $\mathbf{R}$ due to the finite observation can be defined as

$$\hat{\mathbf{R}} = \frac{1}{N}\sum_{k=1}^{N}\mathbf{Y}(k)\mathbf{Y}^H(k). \tag{7}$$

Then, the eigen decomposition of the estimated covariance matrix $\hat{\mathbf{R}}$ which consists of signal and noise subspaces, can be written as

$$\hat{\mathbf{R}} = \hat{\mathbf{U}}_s\hat{\Lambda}_s\hat{\mathbf{U}}_s^H + \hat{\mathbf{U}}_n\hat{\Lambda}_n\hat{\mathbf{U}}_n^H \tag{8}$$

where $\hat{\mathbf{U}}_s$ denote a unitary matrix containing eigenvectors of signal subspace, $\hat{\Lambda}_s$ is a diagonal matrix corresponding to eigenvalues of signal subspace, $\hat{\mathbf{U}}_n$ consists of eigenvectors of noise subspace, and $\hat{\Lambda}_n$ includes eigenvalues of noise subspace. The spatial spectrum of the MUSIC algorithm is obtained by

$$P_{\mathrm{MUSIC}}(\theta) = \frac{\mathbf{a}^H(\theta)\mathbf{a}(\theta)}{\mathbf{a}^H(\theta)\hat{U}_n\hat{U}_n^H\mathbf{a}^T(\theta)}. \tag{9}$$

The direction of arrival from reflected target signals can be obtained by searching the peaks of $P_{\mathrm{MUSIC}}(\theta)$. We implemented the MUSIC algorithm using more than 500 time samples to guarantee the performance of the algorithm in the aspects of both the dependency of time samples and angular accuracy. The performance of angular separation is 10 degree under minimum 10 dB SNR of input signal.

The FMCW waveform and subspace-based DBF algorithm are applied to the long range and narrow angle beam (150 m, $\pm 10^\circ$) of TX antenna #1 as well as the short range and wide angle beam (60 m, $\pm 30^\circ$) of TX antenna #2. The MBMR function of the proposed radar is implemented by the combination of TX switch processing, FMCW control, and DBF algorithm.

3. DESIGN RESULTS

3.1. Front-end Module

Figure 5(a) shows the photograph of designed transceiver module. The TX has an output power of 4 dBm and a VCO phase noise of −94 dBc/Hz at 100 kHz offset. The FMCW signal measured at the TX output port is presented in Figure 5(b). The FMCW signal has 100 MHz bandwidth centered at 24.1 GHz. The RX presents a gain of 28 dB, a noise figure of 13.7 dB, and an IIP3 of −14.5 dBm. The return losses of TX output and RX input have a minimum value of 12.5 dB.

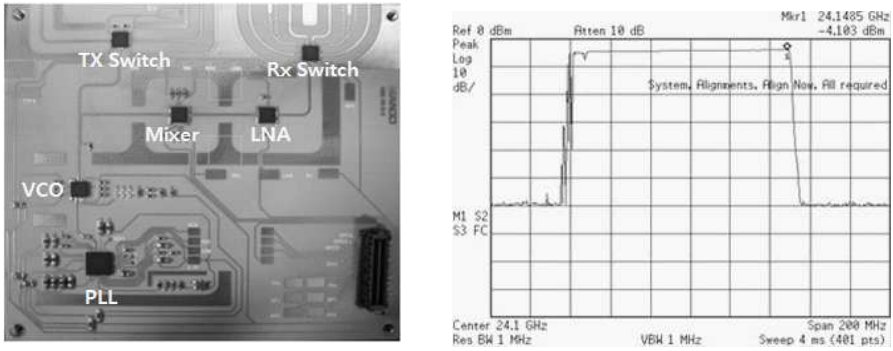

(a) (b)

Figure 5. (a) Photograph of a transceiver module. (b) Measured FMCW signal.

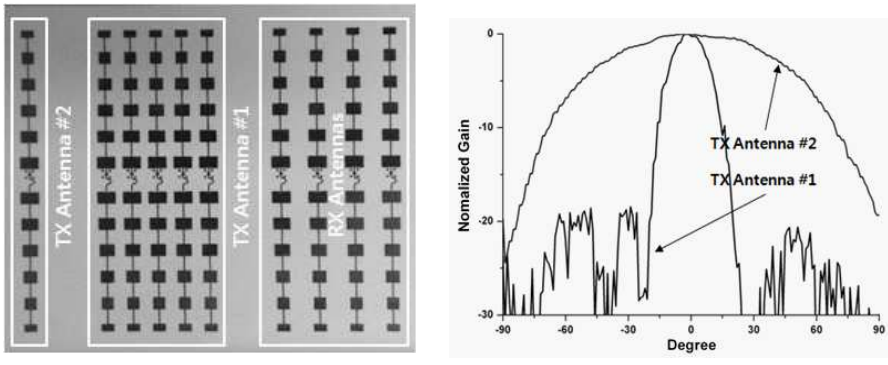

(a) (b)

Figure 6. (a) Photograph of an antenna module. (b) Measured radiation patterns in the azimuth plane.

Table 1. Measured results for front-end module.

Parameter	*Value*
TX antenna #1 gain (dBi)	18
TX antenna #1 SSL (dB)	18
TX antenna #1 HPBW (°)	±10
TX antenna #2 gain (dBi)	15
TX antenna #2 HPBW (°)	±40
TX output power (dBm)	4
VCO phase noise (dBc/Hz @ 100 kHz)	−94
RX gain (dB)	28
RX noise figure (dB)	13.7
RX IIP3 (dBm)	−14.5
TX and RX return loss (dB)	−12.5

Figure 6 shows the design results of an antenna module. The designed array antenna is shown in Figure 6(a). All of the antennas consist of the same one-port linear array. The measured radiation patterns in azimuth plane of the TX antennas are shown in Figure 6(b). The measured results of the azimuth pattern for TX antenna #1 and #2 show gains of 18 dBi and 15 dBi and half-power beam widths (HPBWs) of more than ±10° and ±40° respectively. The side lobe level (SLL) of TX antenna #1 has 18 dB. Each RX antenna has the same results with TX antenna #2 in the aspect of gain and HPBW. The measured main results for the front-end module are summarized in Table 1.

3.2. Back-end Module

Figure 7(a) shows the photograph of designed back-end processing module, which mainly consists of field programmable gate array (FPGA) part and digital signal processor (DSP) part. The FPGA part performs fast multiplication and complex matrix calculation, such as the linear waveform control, coherent acquisition of received beat signals, DBF processing for angle detection, and 1024 fast Fourier transform (FFT) processing of received data. The DSP part performs ordered-statistic constant false alarm rate (OS-CFAR) processing with 10^{-3}, target paring for range and velocity calculation, data association for object grouping, track filtering for rejection of ghost targets, path prediction for primary target selection in the center lane, and vehicle control for stop-and-go.

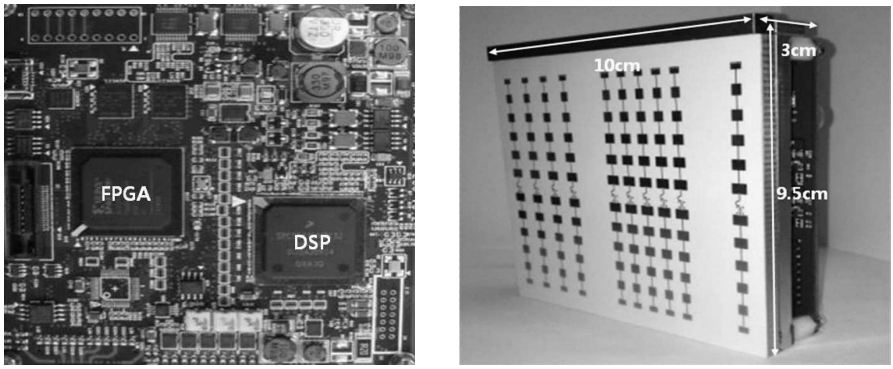

(a) (b)

Figure 7. (a) Photograph of a back-end processing module. (b) Photograph of the proposed MBMR radar.

(a)

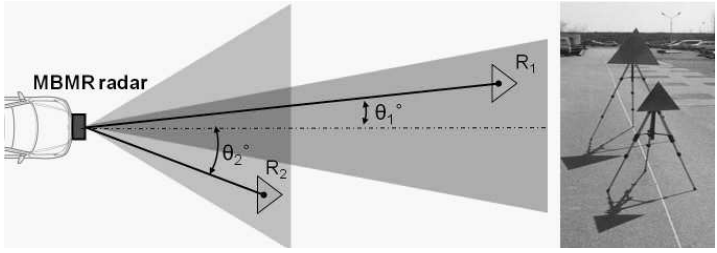

(b)

Figure 8. (a) Vehicle installation of the proposed MBMR radar. (b) Target scenario for measuring the detection performance.

The MBMR radar has a highly integrated size of $10 \times 9.5 \times 3\,\mathrm{cm}^3$ as shown in Figure 7(b). The current consumption of the developed radar module is typically 700 mA with a supply voltage of 12 V.

4. RADAR PERFORMANCE

The proposed MBMR radar was installed in the test vehicle, Tucson ix platform, which is produced by Hyundai Motor Company as shown in Figure 8(a). All of the experiments were performed in an open space on flat ground. Two 10 dBsm target reflectors were used as standard targets for the performance test of the proposed MBMR radar as shown in Figure 8(b). Generally, a 10 dBsm target reflector has almost the same radar cross section (RCS) value as a passenger vehicle.

The experiments were performed to confirm if the MBMR radar could simultaneously detect the range and angle information of two targets, which were located long range and short range beam area, respectively. For the test of the long range and narrow angle beam area, Figure 9 shows that the measured range and angle value of a 10 dBsm target, which was located at the position of 140 m and $-9°$

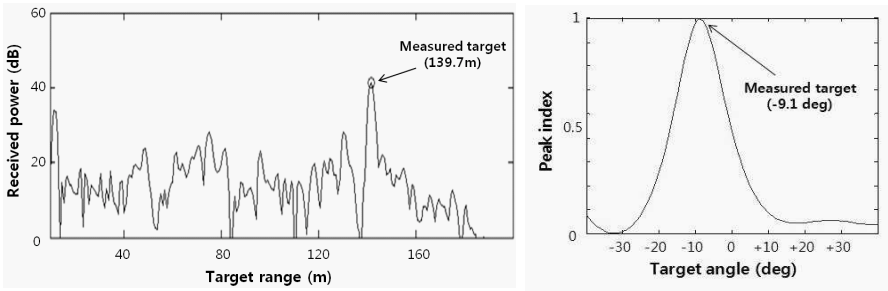

(a) (b)

Figure 9. Measured signal power of a target reflector at the long range and narrow angle beam for (a) range and (b) angle.

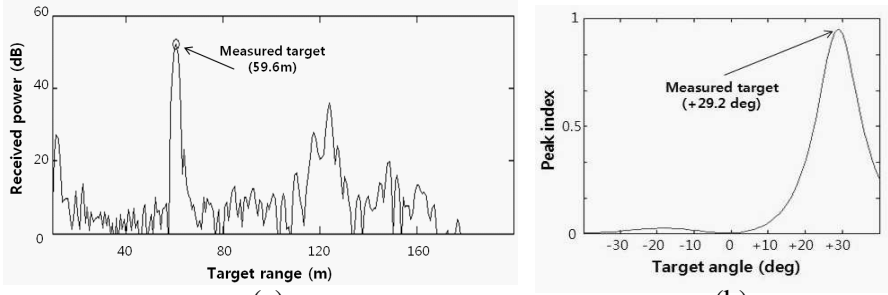

(a) (b)

Figure 10. Measured signal power of a target reflector at the short range and wide angle beam for (a) distance and (b) angle.

were 139.7 m and $-9.1°$. For the test of the short range and wide angle beam area, Figure 10 shows that the measured range and angle value of a 10 dBsm target, which was located at the position of 60 m and $+29°$ were 59.6 m and $+29.2°$. The reflected power of two targets was measured as 42 dB and 53 dB as shown in Figures 9(a) and 10(a), respectively. The power of the detected targets is higher than the noise and clutter around targets.

In this experiment, the two targets which were respectively located at long-narrow beam area and short-wide beam area, were exactly discriminated and detected using two switching array antennas, GaAs RF ICs with low noise figure, equalizer for the enhancement of baseband gain in the long distance area, processing gain from FFT compression, and subspace-based MUSIC algorithm with high resolution and accuracy.

5. CONCLUSION

In this paper, we developed a highly integrated MBMR radar with two-channel TX and four-channel RX using switching array antennas, K-band GaAs RF ICs, FMCW waveform, and subspace based DBF algorithm to overcome the demerits in the aspect of the size and cost of previous radar systems. We demonstrated that the proposed MBMR radar has target detection and target discrimination capabilities of long range beam area (150 m, $\pm 10°$) and short range beam area (60 m, $\pm 30°$) as a single sensor for an ACC stop-and-go application.

REFERENCES

1. Gavrila, D. M., "Sensor-based pedestrian protection," *IEEE Intelligent System*, Vol. 16, No. 6, 77–81, 2001.
2. Russel, M. E., A. Crain, A. Campbell, C. A. Drubin, and W. F. Miccioli, "Millimeter-wave radar sensor for automotive intelligent cruise control (ICC)," *IEEE Trans. Microw. Theory Tech.*, Vol. 45, No. 12, 2444–2453, Dec. 1997.
3. Giubbolini, L., "A multistatic microwave radar sensor for short range anticollision warning," *IEEE Trans. Veh. Technol.*, Vol. 49, No. 6, 2270–2275, Nov. 2000.
4. Wenger, J., "Automotive MM-wave radar: Status and trends in system design and technology," *IEE Colloquium on Automotive Radar and Navigation Techniques*, Feb. 1998.

5. Rasshofer, R. H. and K. Gresser, "Automotive radar and lidar systems for next generation driver assistance functions," *Advances in Radio Science*, Vol. 3, 205–209, 2005.
6. Wilson, T., "IVHS countermeasures for rear-end collisions, task 1: Volume VI — Human factors studies," U.S. Dept. Transportation, Washington, DC, Feb. 1994. [Online]. DOT Rep. HS 808 565. Available: http://www.itsdocs.fhwa.dot.gov/jpodocs/repts_te/45101!.pdf
7. Zechnall, M., "The 'sensitive' automobile-Bosch sensors for complete environmental sensing," Press release, Bosch GMBH, Reutlingen, Germany, Apr. 2001.
8. Rasshofer, R. H. and K. Naab, "77 GHz long range radar systems status, ongoing developments and future challenges," *Radar Conf.*, 2005. http://ieeexplore.ieee.org/stamp/stamp.jsp?arnumber = 01605590.
9. Kawakubo, A., S. Tokoro, Y. Yamada, and T. Kawasaki, "Electronically-scanning millimeter-wave RADAR for forward objects detection," *SAE Congress*, 127–134, 2004.
10. Wixforth, T. and W. Ritschel, "Multimode-radar-technologie für 24 GHz," *Auto Elektronik*, Vol. 3, 56–58, 2004.
11. Gresham, I., et al., "Ultra-wideband radar sensors for short-range vehicular applications," *IEEE Trans. Microw. Theory Tech.*, Vol. 52, No. 9, 2105–2122, Sep. 2004.
12. Jeong, S. H., J. N. Oh, and K. H. Lee, "Design of 24 GHz radar with subspace-based digital beam forming for ACC stop-and-go system," *ETRI Journal*, Vol. 32, No. 5, 827–830, Oct. 2010.
13. Lee, M. S. and Y. H. Kim, "Design and performance of a 24-GHz switch-antenna array FMCW radar system for automotive applications," *IEEE Trans. Veh. Technol.*, Vol. 59, No. 5, 2290–2297, Jun. 2010.
14. Yamaguchi, Y., M. Mitsumoto, M. A. Kawakami, M. Sengoku, and T. Abe, "Detection of objects by synthetic aperture FMCW radar," *Electron. Commun. Jpn. I: Commun.*, Vol. 75, No. 3, 85–94, Mar. 1992.
15. Ishimaru, A. and H. S. Tuan, "Theory of frequency scanning antennas," *IEEE Trans. Antennas Propagat.*, Vol. 10, Mar. 1962.
16. Lange, M., J. Detlefsen, M. Bockmair, and U. Trampnau, "A millimeterwave low-range radar altimeter for helicopter applications — System design," *Conf. Proc. European Microwave Conf.*, 222–227, 1987.

17. Boukari, B., E. Moldvan, S. Affes, K. Wu, R. G. Bosisio, and S. O. Tatu, "A heterodyne six-port FMCW radar sensor architecture based on beat signal phase slope techniques," *Progress In Electromagnetics Research*, Vol. 93, 307–322, 2009.
18. Huang, Y., P. V. Brennan, D. Patrick, I. Weller, P. Roberts, and K. Hughes, "FMCW based MIMO imaging radar for maritime navigation," *Progress In Electromagnetics Research*, Vol. 115, 327–342, 2011.
19. Axelsson, S., "Area target response of triangularly frequency-modulated continuous-wave radars," *IEEE Trans. Aerospace Electron. Syst.*, Vol. 14, 266–277, Mar. 1978.
20. Li, D. D., S. C. Luo, C. Pero, X. Wu, and R. M. Knox, "Millimeter-wave FMCW/monopulse radar front-end for automotive applications," *MTT-S Int. Microwave Symp. Dig.*, 277–280, 1999.
21. O'Halloran, M., M. Glavin, and E. Jones, "Channel-ranked beamformer for the early detection of breast cancer," *Progress In Electromagnetics Research*, Vol. 103, 153–168, 2010.
22. Yang, P., F. Yang, and Z.-P. Nie, "DOA estimation with sub-array divided technique and interporlated ESPRIT algorithm on a cylindrical conformal array antenna," *Progress In Electromagnetics Research*, Vol. 103, 201–216, 2010.
23. Alsehaili, M., S. Noghanian, A. R. Sebak, and D. A. Buchanan, "Angle and time of arrival statistics of a three dimensional geometrical scattering channel model for indoor and outdoor propagation environments," *Progress In Electromagnetics Research*, Vol. 109, 191–209, 2010.
24. Zhang, X., G. Feng, and D. Xu, "Blind direction of angle and time delay estimation algorithm for uniform linear array employing multi-invariance MUSIC," *Progress In Electromagnetics Research Letters*, Vol. 13, 11–20, 2010.
25. Lee, J.-H., Y.-S. Jeong, S.-W. Cho, W.-Y. Yeo, and K. S. J. Pister, "Application of the Newton method to improve the accuracy of toa estimation with the beamforming algorithm and the music algorithm," *Progress In Electromagnetics Research*, Vol. 116, 475–515, 2011.
26. Krim, H. and M. Viberg, "Two decades of array signal processing research," *IEEE Signal Processing Magazine*, Jul. 1996.
27. Chen, Z. and S. Otto, "A taper optimization for pattern synthesis of microstrip series-fed patch array antennas," *IEEE EUWIT*, 160–163, 2009.

28. Musch, T., "A high precision 24-GHz FMCW radar based on a fractional-N ramp-PLL," *IEEE Trans. Instrumentation and Measurement*, Vol. 52, 324–327, Apr. 2003.
29. Bartlett, M. S., "Smoothing periodograms from time-series with continuous spectra," *Nature*, Vol. 161, 686–687, 1948.
30. Schmidt, R. O., "A signal subspace approach to multiple emitter location and spectral estimation," Ph.D. Thesis, Stanford Univ., Stanford, CA, Nov. 1981.
31. Schmidt, R., "Multiple emitter location and signal parameter estimation," *IEEE Trans. Antennas Propagat.*, Vol. 34, 276–280, Mar. 1986.
32. Lee, H. B. and M. S. Wengrovitz, "Resolution threshold of beamspace MUSIC for two closely spaced emitters," *IEEE Trans. Acoustics, Speech, and Signal Processing*, Vol. 38, 1545–1559, Sep. 1990.
33. Li, J., "Improved angular resolution for spatial smoothing techniques," *IEEE Trans. Acoustics, Speech, and Signal Processing*, Vol. 40, 3078–3081, Dec. 1992.
34. Rawiwan, P., P. Satayarak, P. Supanakoon, M. Chamchoy, S. Promwong, and P. Tangtisanon, "Direction-of-arrival estimation using MUSIC and ESPRIT algorithm," *EECON-24*, 682–686, Nov. 2001.
35. Phaisal-atsawasenee, N. and R. Suleesathira, "Improved angular resolution of beamspace MUSIC for finding directions of coherent sources," *IEEE ISSCAA*, 51–56, Harbin, China, Jan. 2006.